

1 New experimental setup for in situ measurement of slow ion induced sputtering

2 P. Salou,¹ H. Lebius,¹ A. Benyagoub,¹ T. Langlinay,¹ D. Lelièvre,¹ and B. Ban-d'Etat^{1, a)}
 3 *CIMAP (CEA-CNRS-ENSICAEN-UCBN), Boulevard Henri Becquerel, BP 5133,*
 4 *14070 Caen Cedex 5, France*

A new experimental equipment allowing to study the sputtering induced by ion beam irradiation is presented. The sputtered particles are collected on a catcher which is analyzed *in situ* by Auger electron spectroscopy without breaking the ultra high vacuum (less than 10^{-9} mbar), avoiding thus any problem linked to possible contamination. This method allows to measure the angular distribution of sputtering yield. Thanks to this new setup it is now possible to study the sputtering of many elements especially light elements such as carbon based materials. Preliminary results are presented in the case of highly oriented pyrolytic graphite and tungsten irradiated by an Ar^+ beam at respectively 2.8 keV and 7 keV.

5 PACS numbers: 79.20.Rf; 34.35.+a; 82.80.Pv

^{a)}bandetat@ganil.fr

6 I. INTRODUCTION

7 Sputtering has been studied for decades, this phenomenon is present in different fields of
8 science and technology such as the cleaning of surfaces, the secondary ion mass spectrometry
9 or the deposition of thin films¹.

10 Sputtering is also an important parameter for the fusion technology. The walls of toka-
11 maks are experiencing an influx of heat and particles from the plasma. The ensuing erosion,
12 which is partially enhanced by chemical reactions, leads not only to a surface modification
13 of the wall elements, but also to the introduction of high-Z materials into the plasma which
14 can contribute to its instabilities. Understanding the reaction between the plasma and the
15 wall materials is thus one of the challenges of the present fusion research².

16 Most of actual tokamak reactors are using carbon based components as wall materials³.
17 This choice is mainly due to their high thermal conductivity, their low Z-value and their
18 capability to sublime instead of melting. However, the hydrogen isotope retention of
19 carbon materials is high compared to other vessel materials like W and Be. In order to
20 respect the tritium inventory limitation⁴, the use of carbon based components in ITER will
21 be restricted only to the deuterium-deuterium fusion reaction. Nevertheless, none of the
22 above-mentioned materials reunites all the advantages of carbon. Therefore, the search for
23 replacement materials is still the subject of intense investigations. The first iteration of wall
24 cladding of the ITER reactor still contains carbon for divertor materials, and a total carbon-
25 free cladding is not planned before 2020. Therefore, besides the search of alternatives, the
26 knowledge on carbon based materials and their interaction with the plasma, in particular
27 sputtering, needs to be improved.

28 Many previous studies on carbon sputtering were performed using plasma immersion⁵.
29 Their application is however limited to basic plasmas, which do not simulate very well the
30 plasma in tokamaks, especially in terms of energy density. An efficient way to study plasma-
31 wall interaction is to simulate the plasma influx by means of ion beams. Contrary to the case
32 of plasma immersion, particle properties are well defined, so the effects of ion species, charge
33 state, energy and flux can be studied separately. It became then possible to extrapolate
34 specific plasma properties. By using ion beam, the erosion can be characterized by the mass
35 loss measured by quartz crystal microbalance⁶. The sputtered particles can also be analyzed
36 by different techniques such as mass spectrometry⁷, or the so-called catcher method⁸⁻¹¹. This

37 last technique has the capability to study neutral species which represent the majority of
38 the sputtered particles.

39 The catcher method was adopted in this work in order to study sputtering by ion beams,
40 specially the sputtering of fusion relevant materials such as carbon based materials. To avoid
41 pollution, like from hydrocarbons present in air, our setup was designed in order to allow an
42 *in situ* analysis of the catcher by Auger electron spectroscopy (AES), in such way that the
43 catcher does not leave the vacuum in-between preparation, irradiation and measurement.

44 II. EXPERIMENTAL SETUP

45 To measure the sputtering yield of graphite induced by ion-surface interactions using the
46 catcher method, the catcher has to stay under ultra high vacuum during all the phases of
47 the experiment. This means that the catcher cleaning by sputtering (Step 1), the irradiation
48 of the target (Step 2) and the catcher analysis (Step 3) have to be performed in the same
49 chamber without breaking the vacuum, implying that the catcher needs to be transferred to
50 different locations. To ensure such a transfer, the catcher is stuck with UHV patches on a
51 belt which can be moved by pulleys as shown in figure 1. Two of them have teeth, allowing
52 to stretch the belt in the vertical way and to rotate it. The catcher can thereby move, facing
53 the different areas (as shown in figure 1). In the area A, the catcher is placed in front of an
54 ion sputter gun for the purpose of cleaning. In the area B dedicated to the irradiation itself,
55 the catcher is bent around the target in order to collect all the sputtered particles produced
56 by ion-surface interaction. Finally the catcher is analyzed in the area C by Auger electron
57 spectroscopy. These different steps are described below.

58 The set-up is placed in a high vacuum chamber, pumped by a dry primary pump and
59 two turbo-molecular pumps in series. After baking at 150°C a pressure below 5.10^{-10} mbar
60 is reached. A gate valve and a collimator are placed between the chamber and the beam
61 line.

62 To collect the sputtered graphite the chosen material for the catcher is silicon, because
63 of its good sticking coefficient, close to one¹². The silicon also allows the analysis by Auger
64 Electron Spectroscopy (AES) since the Auger electron energies of silicon, carbon and oxygen
65 (belonging to the native oxide) are well separated. Moreover, it is possible to get relatively
66 flat Si surfaces and the diffusion coefficient of carbon at this surface is well known¹³. The

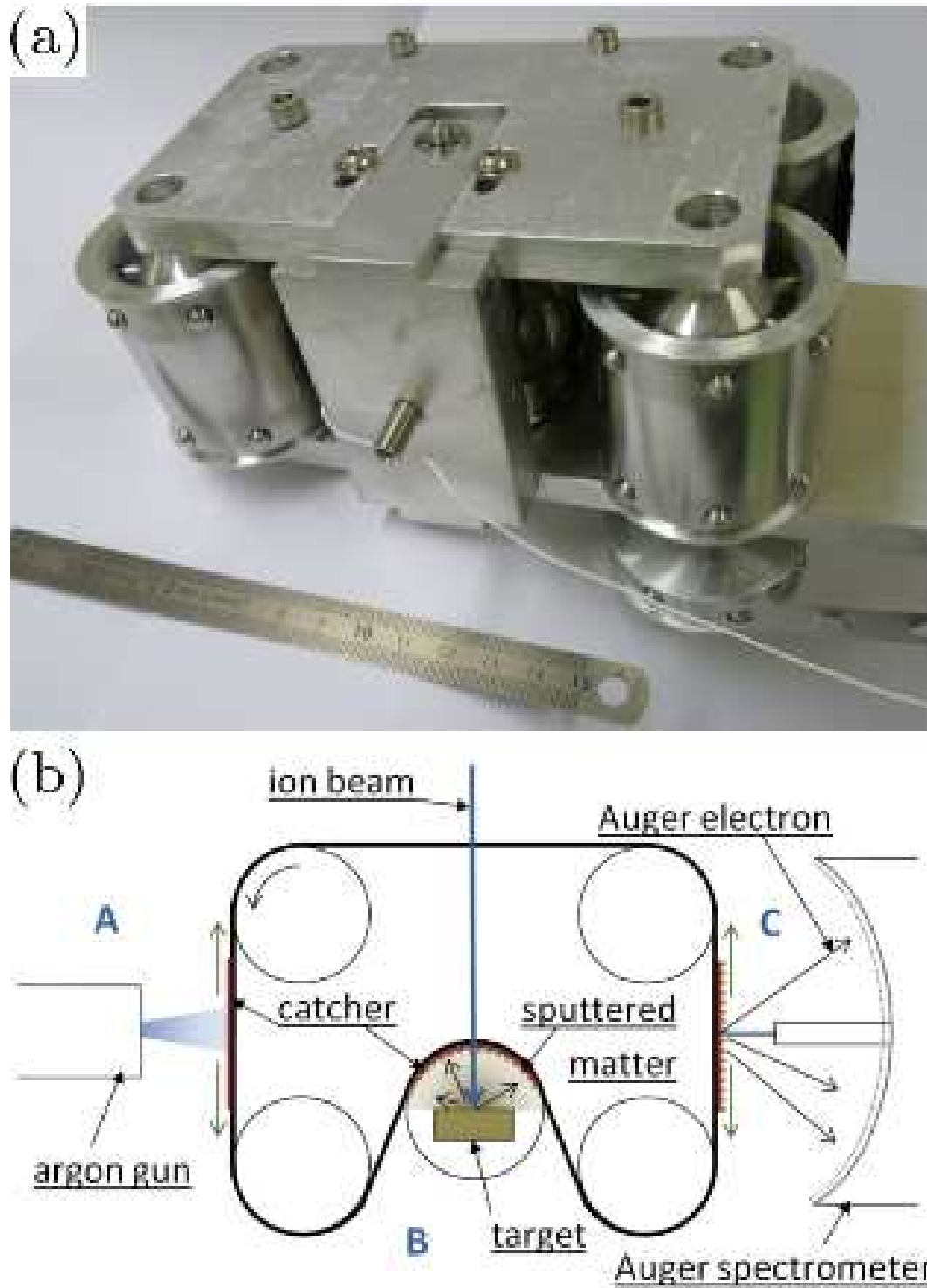


FIG. 1. Overview of the experimental setup : (a) shows the back side of the experimental setup, the beam arrives from the top of the picture, (b) shows a schematic view from the top of the setup.

67 catcher can be made of a thin wafer of silicon, less than 40 μm thick, which can easily be
68 bent. It is then composed of two pieces of $25 \times 5 \text{ mm}^2$ each. The catcher can also be made
69 of several pieces of thicker wafer.

70 The catcher analysis has to be sensitive to very low matter deposition, it is therefore
71 perfectly clean before the sputtering experiment and the analysis by AES which is sensitive
72 to sub-layer deposition. To get an atomically clean surface, a first chemical cleaning is done,
73 the Si catcher is dived for thirty minutes into solvents bathes, respectively trichloroethylene,
74 acetone, methanol and then in pure water. The first bath dissolves grease and hydrocarbons
75 while the other bathes dissolve the previous solvent. A last cleaning is done under vacuum
76 by sputtering using an argon sputter gun. The latter produces single charged ions at 500
77 eV, it is placed at 10 cm from the catcher and at 22° from its normal. The ion beam spot
78 on the catcher is estimated to have a FWHM of 1 cm for an intensity of $0.1 \mu\text{A}$. This last
79 cleaning step is carried on until no pollution is detected by the Auger Spectrometer.

80 Once cleaned, the catcher is transferred to the irradiation area where it is bent around
81 the target in a semi-circular geometry. To get the right belt curvature, an empty pulley,
82 as shown in figure 2, is located in this area. The target is placed in the middle of this
83 pulley and the catcher is positioned at 22 mm from the ion beam impact. The target holder
84 is isolated, so by applying a positive potential to it during ion irradiation, the secondary
85 electrons emitted from the target by incident ions are attracted back to the target allowing
86 thus a precise measurement of the ion beam current. The target holder can host samples
87 with a size up to $25 \times 25 \times 20 \text{ mm}^3$, allowing the study of actual plasma facing materials
88 such as tokamak CFC tiles. The ion beam hits the target after going across the belt through
89 8 mm and 3 mm diameter holes. Just behind the 8 mm hole, a 5 mm and a 4 mm collimators
90 are placed in order to measure the beam current. The target holder can be replaced by a
91 small Faraday cup equipped with a guard ring. For the study of plasma relevant ion beams,
92 noble gases such as He and Ar can be produced by means of filament ion sources. For other
93 elements as H, C, N and O, electron cyclotron resonance sources, such as the Mono1000¹⁴,
94 can be used. To simulate the very low energy particles present in the plasma, this setup can
95 easily be moved to dedicated facilities equipped with low energy beam lines¹⁵ or deceleration
96 lenses⁷.

97 During the irradiation, the sputtered particles are collected on the catcher. Once the
98 desired fluence is reached, the catcher is transferred in front of the Auger spectrometer for



FIG. 2. Target holder.

analysis. The Auger spectrometer is a four-grid retarding field analyzer coupled with a lock-in amplifier (LEED/Auger, OMICRON). The electron beam spot diameter is approximately 0.5 mm. The catcher is scanned all along its length in order to obtain the angular sputtering yield. To deduce the amount of sputtered carbon from the Auger spectrum, we use a prior calibration of the Auger spectrometer which is described in the following paragraph.

III. AES CALIBRATION

Many theoretical models predict the evolution of Auger spectrum as a function of the material composition. In the case of a catcher material collecting another different material we can simulate it by a heterogeneous sample, composed of a substrate of silicon with an upper layer of deposited material. The transition between the condensate and the substrate is assumed sharp. As the analyzing electron spot is rather small, the material can be considered homogeneous all along the surface. Briggs and Seah¹⁶ proposed a simple model to predict the Auger electron intensity of the different elements of the material. In this model the deposited layer is considered flat and uniform. It is thus not completely suited to describe sub-monolayer and film growth modes like that of Volmer-Weber or Stranski-Kratanov¹⁷. However it is well adapted to the description of amorphous carbon film growth. For a condensate C deposited on a substrate S , the amplitude of the Auger electron peak I_C and that of the elastic electron peak I_{EP} follow respectively Eqs. 1 and 2:

$$I_C = k_C I_0 \frac{1 + r_C}{1 + r_S} \{1 - \exp[-d/\Lambda_{C,E_A}]\}, \quad (1)$$

$$I_{EP} = k_{EP} I_0 \{R_C - (R_C - R_S) \exp[-2d/\Lambda_{C,E_{EP}}]\}. \quad (2)$$

117 In these equations I_0 is the primary electron beam intensity and d is the layer thickness.
 118 The constants k_C and k_{EP} depend, among other parameters, on the detector efficiency, the
 119 conversion between the number of electrons and the peak amplitude, and in the case of
 120 Auger electrons on the ionization cross section and the emission probability. The constants
 121 Λ_{C,E_A} and $\Lambda_{C,E_{EP}}$ correspond respectively to the attenuation length of the electrons in the
 122 condensate at the energy of E_A and E_{EP} ; these parameters are linked to the inelastic mean
 123 free path (imfp) ($\lambda_{C,E_{E_A}}$ and $\lambda_{C,E_{EP}}$) through a correction factor, k , taking into account
 124 the elastic collisions and the detector geometry. r_S and r_C correspond respectively to the
 125 backscattering correction factor of the E_A energy electrons in the material substrate and
 126 condensate. R_C and R_S correspond to the backscattering probability of primary electrons
 127 on the condensate and the substrate.

128 In the case of a thin film of carbon covering silicon, r_C and r_S are negligible. To eliminate
 129 any fluctuation of I_0 , it is possible to study the ratio between the Auger and the elastic peaks.
 130 This ratio is given by the following expression:

$$\frac{I_C}{I_{EP}} = \alpha \frac{1 - \exp(-d/\Lambda_{C,E_A})}{R_C - (R_C - R_S) \exp(-2d/\Lambda_{C,E_{EP}})}, \quad (3)$$

131 where $\alpha = [k_C (1 + r_C)] / [k_{EP} (1 + r_S)]$.

132 The above equations include intrinsic and extrinsic parameters. While intrinsic parame-
 133 ters can easily be found in the literature, the extrinsic parameters which are linked to the
 134 Auger spectrometer need to be determined. To measure them we used a setup (described
 135 by Akcöeltekin *et al.*¹⁸) dedicated to sample preparation and post-irradiation analysis. It is
 136 equipped for producing clean surface samples, depositing thin calibrated carbon films, and
 137 analyzing them with the Auger spectrometer.

138 The thin films of carbon were deposited from a graphite rod sublimated by electron
 139 heating. The flux of evaporated particles was measured by using a quartz crystal microbal-
 140 ance located at the sample position. The microbalance was temperature stabilized by water
 141 cooling. During the deposition the stability of the carbon flux was monitored with the
 142 measurement of the intensity of the particle beam.

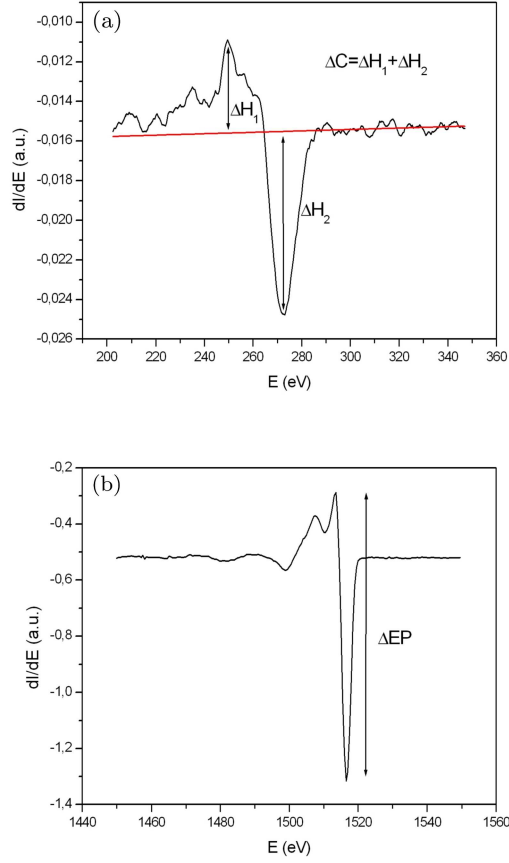


FIG. 3. Intensity measurement of (a) C_{KLL} Auger peak and (b) the elastic peak. $I_C \propto \Delta C$ and $I_{EP} \propto \Delta EP$.

143 The calibration was achieved for silicon samples coated with carbon layers up to 2.8 nm
 144 thick. The Auger spectra were recorded in the derivative mode, the Auger and elastic peak
 145 currents were evaluated from the peak-to-peak height deduced from derived spectra (see
 146 Fig. 3). This method is appropriate to relatively Gaussian shaped peaks (as shown in Ref.
 147 19), which is the case in our study. For the carbon peak we have taken into account the
 148 base-line, as shown in figure 3.

149 During the calibration, the lock-in parameters of the Auger spectrometer were fixed:
 150 modulation amplitude and frequency were respectively 5 Vpp and 4.75 kHz. The time
 151 constant was set to 1 s, the integration time was 2 s and the lock-in used the High Dynamic
 152 Reserve mode.

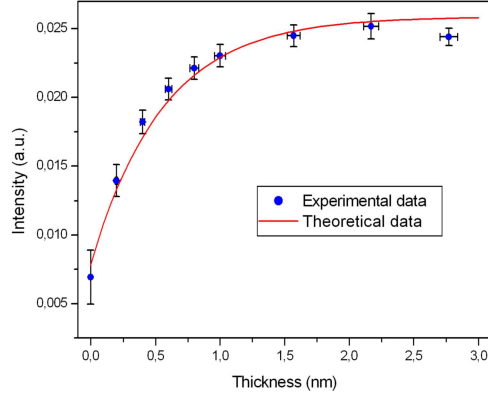


FIG. 4. C_{KLL} Auger peak intensity as a function of the carbon layer thickness.

IV. RESULTS AND DISCUSSION

At this point we observed the same behavior than that described in the Seah's model. However, we did not succeed in getting a clean surface free of carbon and the initial carbon contamination was modeled by a carbon layer of 0.2 nm. By using the impf of C_{KLL} Auger electrons in carbon, $\lambda_{C,EA} = 0.75$ nm, we obtained (Fig 4) a correction factor of $k = 0.74$, which is the value found by Seah²⁰ for such a detector. The relative intensity between the C_{KLL} Auger peak and the elastic peak shows the trend described by Eq. 3. The theoretical curve shown in figure 5 is obtained by using the following parameters: $\lambda_{C,EA} = 0.75$ nm, $\lambda_{C,EP} = 2.09$ nm (for 1.5 keV electrons, according to the universal function given by Seah and Dench²¹), $k = 0.74$, $R_C = 1.7 \cdot 10^{-4}$ and $R_S = 5 \cdot 10^{-4}$ from Ref.22. The fit of Eq. 3 to the experimental data provides $\alpha = 2 \times 10^{-5}$. The measurable can be evaluated to a layer thickness spanning 0 to 1.5 nm.

Different sources of uncertainties can affect this calibration. The two main sources come from the uncertainty on the thickness of the layer and on the intensity of the Auger and elastic peaks. The uncertainty on the thickness of the layer is related to the measurement of the flux and its stability. The quartz crystal micro balance has a systematic error due to the uncertainty on the carbon density and on the geometric configuration. These uncertainties can be neglected. The stability of the flux was estimated to be 2%. The uncertainty on the peak amplitude measurement was obtained by statistics. As the number of Auger spectra is limited by the measurement time, this uncertainty was estimated from the standard devia-

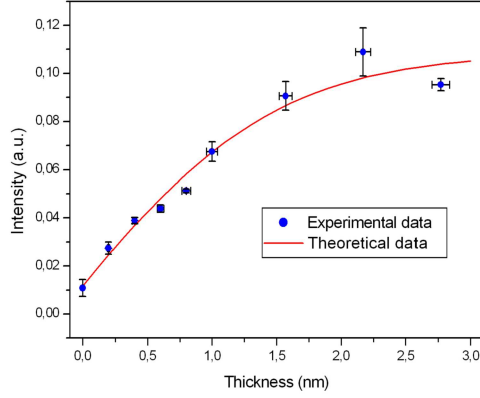


FIG. 5. Ratio of the intensity of C_{KLL} Auger peak and the elastic peak versus the carbon thickness.

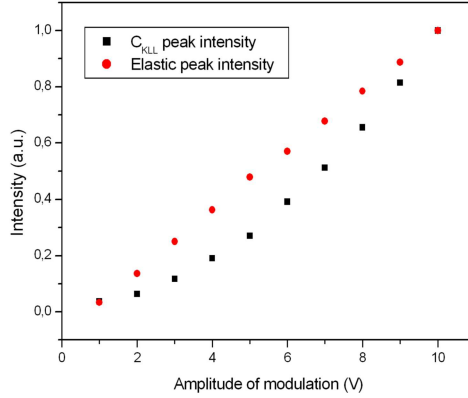


FIG. 6. Normalized intensity of C_{KLL} peak and the elastic peak as a function of the amplitude of modulation of the lock-in detection.

tion of the measurement corrected by a Student factor corresponding to a confidence interval of 70%. As all the measurements were performed by using specific lock-in parameters, the calibration can be considered valid for this set of parameters. However, some parameters such as the modulation amplitude, have to be tuned in order to improve the resolution. A correction factor was then applied to estimate the peak corresponding to a 5 Vpp modulation. Figure 6 shows the evolution of the peak intensities as a function of the amplitude of modulation.

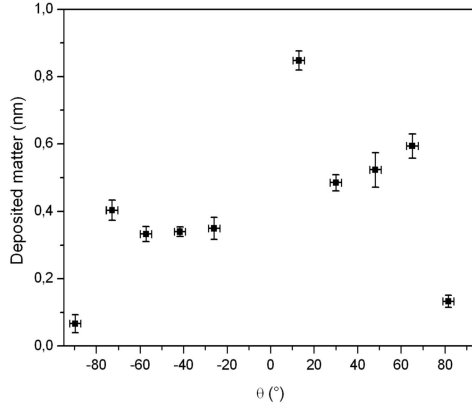


FIG. 7. Distribution of the carbon deposition for a HOPG target irradiated with Ar^+ at 2.8 keV.

V. PRELIMINARY EXPERIMENTS

A set of experiments were performed by irradiating multiple fusion relevant targets. A first experiment was achieved with a target of highly oriented pyrolytic graphite (HOPG) irradiated by an Ar^+ beam of $1 \mu\text{A}$ at 2.8 keV produced by a filament ion source. The target was previously cleaned under atmospheric pressure, and then sputtered under UHV by using the same ion beam than for the experiment. During this phase, the target was electrically biased in order to collect the secondary electrons emitted from the target. The current due to this emission is evaluated to be 10.8%. During the actual sputtering experiment the target was grounded and the ion beam current was deduced analytically. Some extra Si catchers were placed away from the target in order to estimate the pollution during the irradiation. No pollution was detected from these catchers. The catcher analysis started when a fluence of 1.91×10^{18} ions was reached. Figure 7 shows the angular distribution of the deposition thickness, 0° corresponds to the beam incidence. The maximum is reached at around 13° . It corresponds to a deposited carbon layer thickness of about 8.5 \AA . The distribution also shows two shoulders around 70° from the normal. Tripathi et al^{10,11} showed similar results for HOPG irradiated at higher energy (Ag and Au at hundred MeV). They concluded by referring to a crystalline effect leading to preferential angles of sputtering. More data are however necessary to extrapolate such an explanation to lower energies.

A second experiment was performed with a target of tungsten irradiated by an Ar^+ beam of $1.5 \mu\text{A}$ at 7 keV produced by the Mono1000 ion source. The fluence was 4×10^{16} ions. The

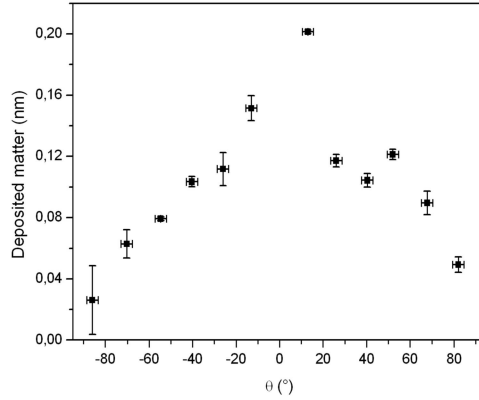


FIG. 8. Distribution of the tungsten deposition for a tungsten target irradiated with Ar^+ at 7 keV.

layer thickness was measured by using Eqs 1 and 2 with the amplitude of the W_{NVV} Auger electron (180 eV) and the elastic peak. Figure 8 shows the distribution of the collected tungsten. The shape of the angular distribution of the sputtering yield exhibits a maximum near the normal incidence and can be described by a cosine law with extra preferential angle around 0° and 50° . This observation was also previously made by Emmoth²³ using similar conditions (tungsten bombarded by Ar^+ at 40 keV).

VI. CONCLUSION AND PERSPECTIVES

An experimental setup that allows the measurement of the angular sputtering yield has been developed. It uses the so-called catcher method to collect sputtered particles, which are then analyzed by Auger electron spectroscopy without leaving the vacuum. This *in situ* measurement allows the study of carbon based materials and other materials like tungsten. The Auger spectrometer was calibrated and preliminary experiments were performed with HOPG and W targets irradiated by an Ar^+ beam, showing an angular yield distribution with preferential angles.

In the future, several experiments are scheduled in order to simulate more closely the irradiation conditions encountered in fusion reactors. For instance, we plan to irradiate various relevant plasma facing materials (such as CFC and W tiles) with very light ions (such as H^+ , D^+ and He^+) at energies of a few hundreds eV. With this setup, it is also possible to study the effect of nitrogen seeding in fusion reactors²⁴.

219 ACKNOWLEDGMENTS

220 We thank the Fédération nationale de Recherche Fusion par Confinement Magnétique
221 for their financial support.

222 REFERENCES

- 223 ¹V. S. Smentkowski, Prog. Surf. Sci. **64**, 1 (2000).
- 224 ²J. Roth, E. Tsitrone, A. Loarte, T. Loarer, G. Counsell, R. Neu, V. Philipps, S. Brezinsek,
225 M. Lehnen, P. Coad, C. Grisolia, K. Schmid, K. Krieger, A. Kallenbach, B. Lipschultz,
226 R. Doerner, R. Causey, V. Alimov, W. Shu, O. Ogorodnikova, A. Kirschner, G. Federici,
227 and A. Kukushkin, J. Nucl. Mater. **390-391**, 1 (2009).
- 228 ³R. Pitts, J. Coad, D. Coster, G. Federici, W. Fundamenski, J. Horacek, K. Krieger,
229 A. Kukushkin, J. Likonen, G. Matthews, M. Rubel, J. Strachan, and J.-E. Contribu-
230 tors, Plasma. Phys. Contr. F. **47**, 303 (2005).
- 231 ⁴G. Federici, C. Skinner, J. Brooks, J. Coad, C. Grisolia, A. Haasz, A. Has-
232 sanein, V. Philipps, C. Pitcher, J. Roth, W. Wampler, and D. Whyte,
233 Nucl. Fusion **41**, 1967 (2001).
- 234 ⁵D. Goebel, Y. Hirooka, R. Conn, W. Leung, G. Campbell, J. Bohdanský, K. Wil-
235 son, W. Bauer, R. Causey, A. Pontau, A. Krauss, D. Gruen, and M. Mendelsohn,
236 J. Nucl. Mater. **145-147**, 61 (1987).
- 237 ⁶F. Aumayr and H. Winter, Philos. T. Roy. Soc. A. **362**, 77 (2004).
- 238 ⁷A. Keim, B. Rasul, N. Endstrasser, P. Scheier, T. D. Mark, and Z. Herman,
239 Int. J. Mass Spectrom. **306**, 204 (2011).
- 240 ⁸S. Bouffard, J. Duraud, M. Mosbah, and S. Schlutig,
241 Nucl. Instrum. Meth. B. **141**, 372 (1998).
- 242 ⁹B. Ban-d'Etat, F. Haranger, P. Boduch, S. Bouffard, H. Lebius, L. Maunoury, J. Y.
243 Pacquet, H. Rothard, C. Clerc, F. Garrido, L. Thomé, R. Hellhammer, Z. Pešić, and
244 N. Stolterfoht, Phys. Scr. **2004**, 389 (2004).
- 245 ¹⁰A. Tripathi, S. A. Khan, S. K. Srivastava, M. Kumar, S. Kumar, S. V. S. N. Rao,
246 G. B. V. S. Lakshmi, A. M. Siddiqui, N. Bajwa, H. S. Nagaraja, V. K. Mittal,
247 A. Szokefalvi, M. Kurth, A. C. Pandey, D. K. Avasthi, and H. D. Carstanjen,

248 Nucl. Instrum. Meth. B. **212**, 402 (2003).

249 ¹¹A. Tripathi, S. A. Khan, M. Kumar, V. Baranwal, R. Krishna, S. Kumar, A. C. Pandey,
250 and D. K. Avasthi, Nucl. Instrum. Meth. B. **266**, 1265 (2008).

251 ¹²J. Roth and C. Hopf, J. Nucl. Mater. **334**, 97 (2004).

252 ¹³F. Pellerin and C. Le Gressus, Surf. Sci. **87**, 203 (1979).

253 ¹⁴C. Pierret, L. Maunoury, S. Biri, J. Y. Pacquet, O. Tuske, and O. Delferriere,
254 Rev. Sci. Instrum. **79**, 02B703 (2008).

255 ¹⁵H. Lebius, A. Brenac, B. A. Huber, L. Maunoury, F. Gustavo, and D. Cormier,
256 Rev Sci Instrum **74**, 2276 (2003).

257 ¹⁶J. E. Castle, *Practical surface analysis by Auger and X-ray photoelectron spectroscopy.*,
258 edited by D. Briggs and M. P. Seah (John Wiley and Sons Ltd, Chichester, 1983).

259 ¹⁷C. Argile and G. E. Rhead, Surf. Sci. Rep. **10**, 277 (1989).

260 ¹⁸S. Akcöltekin, I. Alzaher, B. Ban d'Etat, T. Been, P. Boduch, A. Cassimi, H. Hijazi,
261 H. Lebius, B. Manil, J. M. Ramillon, H. Rothard, M. Schleberger, and E. F. da Silveira,
262 Nucl. Instrum. Meth. B. **267**, 649 (2009).

263 ¹⁹N. J. Taylor, Rev. Sci. Instrum. **40**, 792 (1969).

264 ²⁰M. P. Seah, Surf. Sci. **32**, 703 (1972).

265 ²¹S. Mröz, Prog. Surf. Sci. **46**, 377 (1994).

266 ²²L. Eckertova and C. Kleint, Surf. Sci. **231**, 168 (1990).

267 ²³B. Emmoth, Phys. Scr. **24**, 609 (1981).

268 ²⁴J. Rapp, G. F. Matthews, P. Monier-Garbet, R. Sartori, Y. Corre, T. Eich, R. Fel-
269 ton, W. Fundamenski, C. Giroud, A. Huber, S. Jachmich, P. Morgan, M. O'Mullane,
270 H. R. Koslowski, M. Stamp, and contributors to the Efd-J. E. T. work programme,
271 J. Nucl. Mater. **337-339**, 826 (2005)

272 .